02

Multiple-Band Quasiparticle Transport in Tunneling Junctions Based on Superconducting Stoichiometric $CaKFe_4As_4$ Pnictide

© T.E. Kuzmicheva[1] A.D. Ilina[1] I.A. Nikitchenkov[2,1] K.S. Pervakov[1]
V.A. Vlasenko[1] A.S. Medvedev[1] S.A. Kuzmichev[2,1]

[1] Lebedev Physical Institute, Russian Academy of Sciences, Moscow, Russia
[2] Faculty of Physics, Lomonosov Moscow State University, Moscow, Russia

E-mail: kuzmichev@mig.phys.msu.ru

Received March 6, 2025
Revised March 6, 2025
Accepted May 5, 2025

Using tunneling spectroscopy of planar „break-junctions“ we show a multiple-gap superconductivity in $CaKFe_4As_4$ pnictides. We determine the magnitudes and temperature dependences of the microscopic superconducting order parameter $\Delta_i(T)$. The temperature dependences of the features caused by Andreev transport are obtained: Andreev excess current $I_{exc}(T)$ and Andreev zero-bias conductance $G^{A}_{ZBC}(T)$. As well, the temperature dependence of the critical current $I_c(T)$ is measured. Using data of $I_{exc}(T)$, $G^{A}_{ZBC}(T)$, and $I_c(T)$, we estimate the partial conductance of the two effective bands, and show the dominate contribution of the „driving“ bands with the large superconducting gap to the total conductance.

Keywords: high-temperature superconductivity, pnictides, tunneling spectroscopy, multiple Andreev reflections, superconducting order parameter.

DOI: 10.61011/PSS.2025.07.61874.9HH-25

1. Introduction

Superconductors of the newly discovered 1144 type family based on alkali metals of general composition $XYFe_4As_4$ (where X is an alkaline earth metal or rare earth Eu, Y is an alkali metal) [1] seem to be very promising for applied and fundamental research (for an overview, see Ref. [2]). A typical representative of this family $CaKFe_4As_4$ has a layered crystal structure consisting of a stack of antifluorite-like superconducting (SC) FeAs blocks with a tetragonal lattice in ab-plane divided along c-directions by alternating Ca and K planes [1]. The presence of alkali metal atoms in the structure provides hole „self-doping“ of FeAs SC blocks, which, unlike most iron pnictides, contributes to the development of superconductivity precisely in the stoichiometric composition, with the maximum critical temperature for this compound of $T_c \approx 35\,K$, as well as the absence of magnetism and nematic order of higher than T_c [1].

Calculations of the band structure [3] have shown that the Fermi level in $CaKFe_4As_4$ intersects about 10 bands, forming several nested, weakly corrugated along k_z-direction hole cylinders of the Fermi surface around Γ-point of the Brillouin zone and several electronic cylinders around the M-point. A SC condensate with different coupling energies of Cooper pairs is formed on each sheet of the Fermi surface below T_c, according to calculations, i.e., 10-gap superconductivity is formally realized. Three hole pockets at the Γ-point and $1-2$ electronic pockets at the M-point are confidently identified in the studies using angle-resolved photoemission spectroscopy (ARPES) [4,5]. The four SC order parameters realized on the Fermi surface cylinders detected with the help of APRES had rather high characteristic ratios $2\Delta_i(0)/k_BT_c \approx 5-9$ exceeding the weak coupling limit of 3.53, which is consistent with the optical [6] and femtosecond spectroscopy [7].

In experiments using scanning tunneling spectroscopy (STS) [5,8,9,10] and point contact spectroscopy (PC) [11], fairly wide maxima were observed in the spectra of tunneling and Andreev contacts at $T \ll T_c$ in the bias ranges of $|V_S| \approx 3-4\,mV$ and $|V_L| \approx 6-8\,mV$, interpreted by the authors of these papers as gap features from small and large SC-gaps. Unfortunately, it is not possible to accurately estimate the amplitudes of Δ_i based on these data due to the strong smearing: the authors of Refs. [5,8,10,11] managed to satisfactorily approximate the experimental data only by introducing a monstrous spread of values $\Delta_i(0)$ from 0 to $\sim 10-12\,meV$, corresponding to 100 % anisotropy in real space, i.e., multiphase and complete chaos of properties.

Our preliminary spectroscopy studies of the incoherent multiple Andreev reflections effect (IMARE), conducted at $T \ll T_c$, showed the coexistence of three bulk SC order parameters with characteristic ratios averaging $2\Delta_i(0)/k_BT_c \approx 5.6$, 3.9 and 1.3.

The temperature dependence of the concentration of Cooper pairs $\rho_S(T)$ was obtained using measurements of the London penetration depth [8,11,12] and muon spectroscopy [13]. A significant „curving down“ was observed in the dependencies at temperatures $T \approx 10-15\,K$. To

fit this feature, in addition to a large superconducting gap with $2\Delta_i(0)/k_BT_c \approx 6-9$ (which agrees with the data from Refs. [4–11]), the introduction of a smaller superconducting order parameter Δ_S with $2\Delta_S(0)/k_BT_c \approx 1-2$ is required [8,11,12,13].

The SC properties of polycrystalline $CaKFe_4As_4$ samples were studied in this paper using two complementary methods. The amplitudes of the SC order parameters and their temperature dependences are directly determined using IMARE spectroscopy. The dependences of the features caused by the multiple-band Andreev transport are obtained: the dependence of the Andreev excess current $I_{exc}(T)$ and the Andreev zero-bias conductance $G^A_{ZBC}(T)$ in the $I(V)$ and $dI(V)/dV$-characteristics of the Andreev contacts; the partial conductances of the effective bands are estimated based on their analysis within the framework of the multiple-band approach. Such data are not available in the literature at the moment. Tunneling spectroscopy was used to measure the temperature dependence of the supercurrent $I_c(T)$ for SC constrictions, which is proportional to the concentration of Cooper pairs $\rho_S(T)$. It is shown that $I_c(T)$ data can be described within the framework of theoretical concepts using the data $\Delta_i(T)$ measured directly by IMARE spectroscopy.

2. Details of the experiment

Polycrystalline $CaKFe_4As_4$ samples were synthesized from pre-prepared precursors CaAs, KAs, and Fe_2As in a molar ratio 1:1:2. The initial reagents used were Ca(99.9 %), K(99.95 %), Fe(99.98 %) and As(99.9999 %). The resulting precursors were ground and mixed in an agate mortar. The powder was poured into a corundum crucible, which was brewed into a niobium container. The container was placed in a vacuum furnace and calcined in an argon atmosphere at a temperature of 955 °C for 6 hours. The resulting powder was ground in an agate mortar and pressed into tablets with a diameter of 12 mm under a pressure of 10 MPa. The tablets were placed in a niobium container and brewed using argon arc welding in an argon atmosphere. The container was placed in a vacuum furnace and calcined at a temperature of 955 °C for 6 hours in an argon atmosphere. All synthesis operations, except calcination, were carried out in a glove box in an argon atmosphere with an oxygen and water content of less than 0.1 ppm.

As a result, dense polycrystalline samples were obtained, which were crushed in an agate mortar for X-ray phase analysis. According to the XRD data, the samples are single-phase, the lattice parameters were refined by the Le Bail method and determined as $a = 3.8534(12)$ Å, $c = 12.830(5)$ Å.

The methods of tunneling spectroscopy of superconductor-constriction-superconductor (ScS) contacts and IMARE spectroscopy of SnS contacts (where n is a thin normal metal) were used to study quasiparticle transport in the SC and the normal state.

In a low-capacitance ScS-contact with a size $d < 2\xi_0$ (where ξ_0 is the coherence length) and with the overlap of the wave functions of the SC condensates inside the tunneling barrier, a vertical supercurrent branch is present in the current-voltage characterisitc (CVC) at a bias $eV = 0$ below T_c. The amplitude of the supercurrent I_c is determined by the temperature dependence of the SC order parameter $\Delta(T)$ according to the Ambegaokar-Baratoff formula [14] and is proportional to the concentration of Cooper pairs $\rho_S(T)$ from the BCS theory

$$I_c(T) = \frac{\pi}{2}\frac{\Delta(T)}{eR_N}\tanh\frac{\Delta(T)}{2k_BT} \propto \rho_s(T). \quad (1)$$

When the critical current I_c is exceeded (using a DC source), a horizontal „jump“to a quasiparticle branch is observed in the CVC. The following can be written in the two-band approximation

$$\frac{I_c(T)}{I_c(0)} = \omega\delta_L(T)\tanh\frac{\Delta_L(T)}{2k_BT} + (1-\omega)\delta_S(T)\tanh\frac{\Delta_S(T)}{2k_BT},$$

$$\delta(T) \equiv \frac{\Delta(T)}{\Delta(0)}, \quad (2)$$

where $R_N \equiv 1/G_N$ is the normal contact resistance at $eV \gg 2\Delta(0)$, and the weight contribution of the band with a large SC gap is

$$\omega = \frac{G_L\Delta_L(0)}{G_L\Delta_L(0) + G_S\Delta_S(0)}. \quad (3)$$

The IMARE effect is realized below T_c in a superconductor-thin normal metal-superconductor (SnS) contact with dimensions $l > d > \xi_0$ (where l is the characteristic inelastic scattering length) and, consequently, a lack of phase coherence between the superconducting banks [15–18]. There is no supercurrent branch at $eV = 0$ in the CVC of an SnS-contact. However, in the case of high tunneling barrier transparency ($T > 80$ %, corresponding to a barrier parameter $Z < 0.5$), a region of increased slope (the so-called „foot“) is observed: the zero-bias conductance G_{ZBC} is finite but can be several times higher than G_N [16–18]. The Andreev excess current $I_{exc}(V,T) \equiv I(V,T) - I(V,T_c)$ is observed over the entire bias range, tending to a constant value at $eV \gg 2\Delta(0)$ [15,16]. For an „ideal“ contact (with $Z = 0$ and the broadening parameter $\Gamma = \hbar/(2\tau) = 0$, τ is the characteristic time of inelastic electron scattering) based on a single-band classical superconductor, the temperature dependences of the Andreev excess current $I_{exc}(T)$ at $eV \gg 2\Delta(0)$ and Andreev zero-bias conductance $G^A_{ZBC}(T) \equiv (G_{ZBC}(T)/G_N - 1)$ is determined by the dependence of the SC gap $\Delta(T)$ [15,19,20]:

$$I_{exc}(T) = \frac{8}{3}\frac{G_N}{e}e^{-\frac{d}{l}}\Delta(T)\tanh\frac{eV}{2k_BT}, \quad (4)$$

$$G^{\mathrm{A}}_{\mathrm{ZBC}}(T) = G_{\mathrm{N}}\,\frac{l}{d}\,\tanh\,\frac{\Delta(T)}{2k_{\mathrm{B}}T}. \quad (5)$$

Due to the large number of unknown parameters of the real contact (d, l, Z, Γ), it is difficult to estimate them from the experiment based on the analysis of absolute values $I_{\mathrm{exc}}(T)$ and $G^{\mathrm{A}}_{\mathrm{ZBC}}(T)$. Nevertheless, it is possible to study the temperature trends of these values. In the two-band approximation, normalized formulas (4), (5) can be written as [21]

$$\frac{I_{\mathrm{exc}}(T)}{I_{\mathrm{exc}}(0)} = \varphi\delta_{\mathrm{L}}(T) + (1-\phi)\delta_{\mathrm{S}}(T),\ \ \delta(T) \equiv \frac{\Delta(T)}{\Delta(0)}, \quad (6)$$

$$\frac{G^{\mathrm{A}}_{\mathrm{ZBC}}(T)}{G^{\mathrm{A}}_{\mathrm{ZBC}}(0)} = \chi\,\tanh\,\frac{\Delta_{\mathrm{L}}(T)}{2k_{\mathrm{B}}T} + (1-\chi)\tanh\,\frac{\Delta_{\mathrm{S}}(T)}{2k_{\mathrm{B}}T}. \quad (7)$$

The weight coefficient χ of the dependence $G^{\mathrm{A}}_{\mathrm{ZBC}}(T)$ corresponds to the partial normal conductance G_{L} of the band with a large SC gap [21]

$$\chi = \frac{G_{\mathrm{L}}}{G_{\mathrm{N}}} \equiv \frac{G_{\mathrm{L}}}{G_{\mathrm{L}} + G_{\mathrm{S}}}, \quad (8)$$

in this case, the weight coefficient ϕ of the dependence $I_{\mathrm{exc}}(T)$ is approximately equal to

$$\varphi \approx \frac{G_{\mathrm{L}}\Delta_{\mathrm{L}}(0)}{G_{\mathrm{L}}\Delta_{\mathrm{L}}(0) + G_{\mathrm{S}}\Delta_{\mathrm{S}}(0)}. \quad (9)$$

The partial conductance of a band with a large SC gap can be estimated from the $I_{\mathrm{exc}}(T)$ data (i. e., the value χ_{exc}) or from the $I_{\mathrm{c}}(T)$ data (value χ_{Ic}) as [21]

$$\chi_{\mathrm{exc}} \approx \left[\left(\frac{1}{\varphi} - 1\right)\frac{\Delta_{\mathrm{L}}(0)}{\Delta_{\mathrm{S}}(0)} + 1\right]^{-1}. \quad (10)$$

In the dynamic conductance spectrum of a high-transparency SnS contact, IMARE causes the occurrence of a subharmonic gap structure (SGS) [15,16]: minima $dI(V)/dV$ at bias voltages

$$\mathrm{eV}_n(T) = \frac{2\Delta(T)}{n}, \quad (11)$$

where n is a natural number. According to Ref. [16], the position V_n of Andreev minima is directly determined by the magnitude of the SC gap $\Delta(T)$ at any temperatures up to T_{c}. For an SnS contact based on a multiple-gap superconductor, several SGS are expected to appear on the $dI(V)/dV$-spectrum, the position of which corresponds to $\Delta_i(T)$. For $T \to 0$, the number of n^* minima observed on $dI(V)/dV$ in the spectrum of the planar SnS contact for each band (for the case Z, $\Gamma = 0$) approximately corresponds to the ratio l/d along the crystallographic c-direction [16], as well as the ratio of Andreev zero-bias conductance to the normal one [19,20] $n^* \approx l/d \approx G^{\mathrm{A}}_{\mathrm{ZBC}}/G_{\mathrm{N}}$ and decreases in real contact with small but non-zero Z [15] and Γ.

The study of planar SnS contacts with ballistic transport ($d < l^{\mathrm{el}}$ along the ab-plane, where l^{el} is the mean free path) allows obtaining information about the possible anisotropy of the SC gap in the k_xk_y-plane pulse space. According to calculations [22], the shape of the Andreev features of the SGS may vary depending on the type of symmetry of the SC order parameter. Sharp intense minima are expected in the $dI(V)/dV$-spectrum of the SnS contact based on an isotropic gap superconductor (s-wave symmetry). At the same time, the amplitude of the features is suppressed in the case of the anisotropy of the SC gap in k-space ($\Delta(\theta)$ angle distribution, where θ is the direction of the momentum): for a gap with nodes (for example, d-wave symmetry), the amplitude of the SGS minima does not exceed $\sim (5{-}10\,\%)G_{\mathrm{N}}$ [22]. Numerical calculations using the approach in Ref. [22] have shown that for the case of extended s-wave symmetry of the SC gap without nodes (spectrum № 2 in Figure 4 in Ref. [23]), extended features are expected representing doublets consisting of two minima connected by an „arch“. The position of the minima is directly determined by the maximum (Δ^{out}) and minimum (Δ^{in}) coupling energies of the Cooper pairs, depending on the direction of the momentum. The degree of anisotropy is further estimated as $\mathrm{A} \equiv 100\,\% \cdot [1 - (\Delta^{\mathrm{in}}/\Delta^{\mathrm{out}})]$.

Tunneling structures of the above types were created using the „planar mechanically adjustable break-junction“ [23] technique, which is a modification of the classic „break-junction“ [24] technique applied to layered compounds. The specifics of the configuration used, the advantages and disadvantages of the method are discussed in detail in the review in Ref. [23].

A sample prepared in the form of a rectangular plate with a size of $3 \times 1.5 \times 0.3\,\mathrm{mm}^3$ was mounted using liquid In-Ga solder at room temperature, 4 contacts were applied, which fixed the sample on a springy Π-shaped holder made of beryllium bronze. Next, the sample holder was cooled to $T = 4.2\,\mathrm{K}$ and bent precisely, which contributed to the splitting of the sample. The formation of microcracks was monitored in real time by the appearance of the final slope of the cracked sample.

In the general case, the microcrack separating two massive SC-banks is a superconductor-constriction-superconductor (ScS) type structure. During the experiment, the crack remains „closed“, i. e., the parts of the sample are not separated by a significant distance, unlike the classical technique. This protects the cryogenic cleft from degradation and penetration of impurities, which makes it possible to obtain high-quality tunneling contacts and observe a bulk SC gap that is not affected by surface effects. By fine-tuning, varying the bending of the table, it is possible to change the point of contact and obtain dozens of tunneling contacts on the same sample, which is necessary to set statistical data and verify the reproducibility of certain values of the SC gap. Depending on the transparency and thickness of the barrier, various spectroscopy methods can be implemented on the break-junction contacts.

In the general case, cleavage in polycrystalline samples runs along the grain boundaries. However, as we showed earlier [23], in polycrystalline samples of *layered*

compounds, when the grain bonding strength exceeds the interlayer bond, it is possible to split individual crystalline grains in which the crystallographic ab-planes are oriented along the crack. Steps and terraces characteristic of any layered compounds are observed on the surface of such split grains (Figure 2 in [23]), on which planar ScS contacts with current flow along the crystallographic c-direction can be obtained. According to our estimates, for single and polycrystals of related layered compounds [23,25,26], the size of the contact region is about 10–50 nm is much smaller than the average width of the terrace ($\sim$ 100–500 nm) and the size of crystalline grains (up to 1 μm). For planar contact, the IMARE observation condition must be fulfilled along the c-direction ($l_c > d_c$). The dependence of the coupling energy of Cooper pairs on the momentum direction can be resolved in the k_xk_y-plane under the condition of ballistic flight of quasiparticles $l_{ab}^{el} > d_{ab}$, while along the k_z-direction there is „mixing“ charge carriers and averaging of $\Delta(k_z)$ [23].

3. Results

Figure 1 shows the CVC (orange line, right vertical axis) and the corresponding $dI(V)/dV$-spectrum (red line, left axis) of the SnS contact on a microcrack obtained with $T = 3.1\,\mathrm{K} \ll T_c$ in a polycrystalline $CaKFe_4As_4$ sample. The CVC is almost symmetrical with respect to zero, does not contain „jumps“ and hysteresis. There is no supercurrent branch on the CVC at eV = 0, instead, it shows a region of increased slope, so called „foot“. Over the entire bias range, this CVC passes above the normal-state one of the same contact, measured at $T = 36\,\mathrm{K} > T_c$ (dashed line), i.e. it has an excess current. The slopes of the CVC measured below and above T_c approximately coincide at large biases, i.e., the Andreev excess current tends to a constant value. These features of the CVC clearly indicate the realization of an IMARE regime of high transparency in accordance with all available theoretical concepts [15–20]. The observed $I_{exc}(V) \to$ const at large bias eV $\gg 2\Delta(0)$ also corresponds to the approximate constancy of the normal resistance $R_N(T) \to$ const with temperature, which indicates the absence of local overheating and the implementation of ballistic quasiparticle transport through the contact.

The corresponding $dI(V)/dV$-spectrum has sharp minima at biases of approximately 17.4, 12.2, and 8.7 mV (the blue and pink lines in Figure 1), which do not correspond to the formula (11) and cannot belong to the same SGS of the isotropic gap. The spectrum is rather smooth at $|V| > 18$ mV. Assuming each of the two minima located at the maximum bias $|\Delta_{1L}^{out}| \approx 17.4$ mV and $|\Delta_{1L}^{in}| \approx 12.2$ mV, as a doublet from the fundamental Andreev harmonic ($n_i = 1$), it is possible to directly determine the two characteristic coupling energies of Cooper pairs $2\Delta_L^{out}(0) \approx 17.4$ meV and $2\Delta_L^{in}(0) \approx 12.2$ meV, corresponding to the anisotropic distribution of the gap

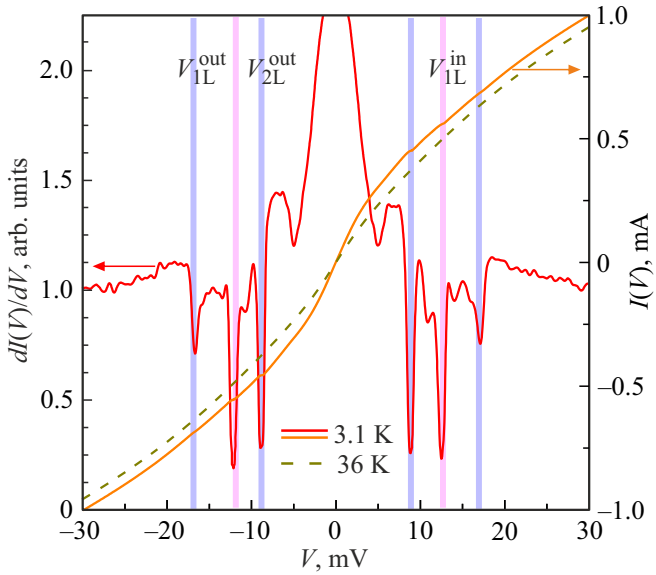

Figure 1. CVC (right vertical axis) and $dI(V)/dV$-spectrum (left axis) of the SnS-Andreev contact in a polycrystalline sample of layered pnictide $CaKFe_4As_4$, measured at $T = 3.1\,\mathrm{K} \ll T_c$. The position of the fundamental (n = 1) harmonic Δ_{1L}^{out} and the second (n = 2) subharmonic Δ_{2L}^{out} from the SC order parameters $2\Delta_L^{out}(0) \approx 17.4$ meV is marked by vertical blue lines, the fundamental harmonics Δ_{1L}^{in} of the SC order parameter $2\Delta_L^{in}(0) \approx 12.2$ meV — pink lines. The CVC of the same contact obtained above T_c (dashed line) is shown for comparison.

in k-space. The minimum located at half the bias $|\Delta_{2L}^{out}| \approx |\Delta_{1L}^{out}|/2 \approx 8.7$ mV, can be interpreted as the second (n = 2) subharmonic of Δ_L^{out}. The second subharmonic from Δ_L^{in}, expected at $|\Delta_{2L}^{in}| \approx 6.1$ mV, approximately overlaps with the beginning of the foot (corresponding to the minimum of $dI(V)/dV$ at $|V| \approx 5.3$ mV) and probably for this reason is not allowed as a separate a feature.

The temperature evolution of the $dI(V)/dV$-spectrum of the SnS contact in Figure 1 is shown in Figure 2, a. As noted above, the normal contact resistance remains approximately constant with increasing temperature, however, for the convenience of considering Andreev structures, the spectra in Figure 2, a are manually shifted vertically. As the temperature increases, the amplitude of all the Andreev features, as well as the foot height G_{ZBC}, decreases, and their position shifts towards zero. At $T = 33.8$ K (the upper curve in Figure 2), the spectrum is smoothed out and has no Andreev features, which means the absence of Cooper pairs and the transition of the contact region to a normal state, determining its local critical temperature T_c^{local}.

The dependence of the positions of the main features of dynamic conductance on temperature according to Figure 2, a is shown in Figure 2, b. The features at Δ_{1L}^{out} and Δ_{2L}^{out} (solid and open circles) have similar temperature behavior, and their position differs approximately twice over the entire temperature range up to T_c, as shown in the upper inset to Figure 2, b. This confirms the earlier conclusion

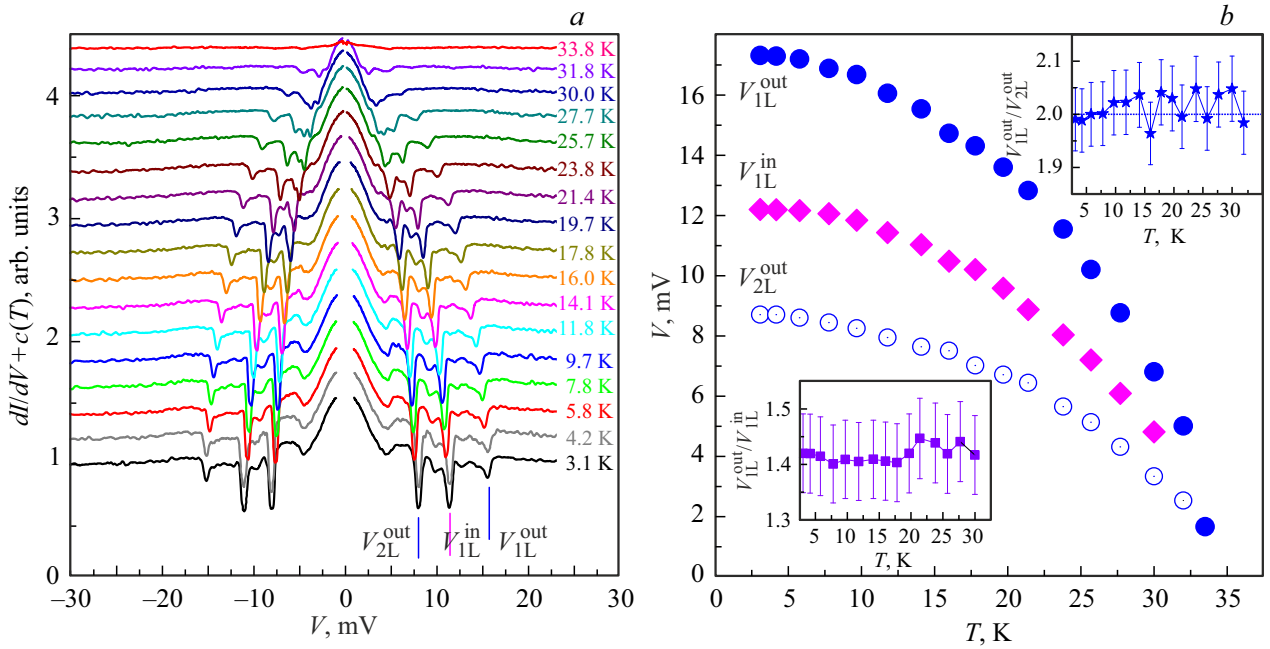

Figure 2. *a* — $dI(V)/dV$-spectrum of the SnS-Andreev contact (shown in Figure 1), measured at $T = 3.1-33.8$ K. For convenience, $dI(V)/dV$ are normalized to the corresponding spectrum at $T > T_c$ and manually shifted vertically. Vertical dashes at $T = 3.1$ K mark the position of the Andreev harmonics Δ_{1L}^{out}, Δ_{2L}^{out} and Δ_{1L}^{in}. *b* — temperature dependences of the positions of the Andreev features Δ_{1L}^{out} and Δ_{2L}^{out} (dark and light circles), Δ_{1L}^{in} (diamonds). The upper insert shows the ratio of the bias of the first and second Andreev features $\Delta_{1L}^{out}/\Delta_{2L}^{out}$ depending on the temperature, the lower insert shows the ratio $\Delta_{1L}^{out}/\Delta_{1L}^{in}$.

that the feature at Δ_{2L}^{out} is the second subharmonic of Δ_{1L}^{out}, directly determining the dependence of the same SC order parameter $2\Delta_L^{out}(T)$ on temperature. At the same time, the feature at the offset Δ_{1L}^{in}, which determines the dependence $2\Delta_L^{in}(T)$, also has a similar temperature trend: the ratio $\Delta_L^{out}(T)/\Delta_L^{in}(T)$ remains approximately constant in the range from $T = 3.1$ K to T_c (bottom insert in Figure 2, *b*). The temperature course of the minimum at small bias voltages $|V(0)| \approx 5.3$ mV generally repeats the shape of the dependences of the Andreev features on $\Delta_L^{out}(T)$ and $\Delta_L^{in}(T)$, therefore this feature can be interpreted as the beginning of a pedestal, rather than the fundamental harmonic from a small SC gap.

Doublet Andreev features (two closely located minima) with a similar temperature evolution ($\Delta_L^{out}(T)/\Delta_L^{in}(T) \approx$ const) are reproducibly observed by us on $dI(V)/dV$-spectra of SnS contacts in iron-containing superconductors $EuCsFe_4As_4$ of the related family 1144 [27,28], $Ba(Fe,Ni)_2As_2$ of the 122 isostructural family [25], as well as in the alkali metal-based pnictides LiFeAs and Na(Fe,Co)As [29,30]; on the contrary, it was not reproducibly observed, for example, in the oxypnictides of the 1111 system [26]. In general, we can suggest two scenarios for the appearance of such doublets.

1. The presence of two isotropic SC gaps Δ_L^{out} and Δ_L^{in} opening on different sheets of the Fermi surface, the magnitudes of which differ by 1.3–1.5 times. According to the classical BCS-like multiple-band approach — the system of Moskalenko and Suhl equations [31,32] — the constancy of the ratio Δ_1/Δ_2 over the entire temperature range is realized in the unique case of the zero determinant of the matrix of coupling constants λ_{ij}. Although such a scenario cannot be ruled out for a specific superconductor, its simultaneous realization in pnictides of three families [25,27–30] seems unlikely.

2. The presence of a single SC condensate with anisotropy of the order parameter Δ_L depending on the momentum direction. In this case, the two minima on the $dI(V)/dV$-spectrum represent a single extended feature (doublet), and the characteristic energies Δ_L^{out} and Δ_L^{in} correspond to the extremes of the angular distribution $\Delta_L(\theta)$ in k_xk_y-plane.

3. Emission of a quasiparticle with energy $\varepsilon_1 = \Delta_L^{out} - \Delta_L^{in}$ will create a second minimum (with higher energy) for those Andreev electrons that emitted this quasiparticle and loose energy ε_1 in the IMARE process. In this case, ε_1 may have its own, weaker dependence on T, unrelated to $\Delta(T)$. Then, for $T \to T_c$, we get a very different ratio of the positions of the features of $\Delta_L^{in}/\Delta_L^{out} \to 0$, which is not observed in our case.

Figure 3, *a* shows the temperature behavior of $dI(V)/dV$-spectrum of another SnS contact obtained in polycrystalline $CaKFe_4As_4$ sample from the same batch. A doublet of the fundamental Andreev harmonic containing minima of dynamic conductance at $|\Delta_{1L}^{out}(0)| \approx 17$ mV and $|\Delta_{1L}^{in}(0)| \approx 10$ mV (blue and purple vertical dashes) can be seen at $T = 4.2$ K $\ll T_c$ (lower curve in Figure 3, *a*).

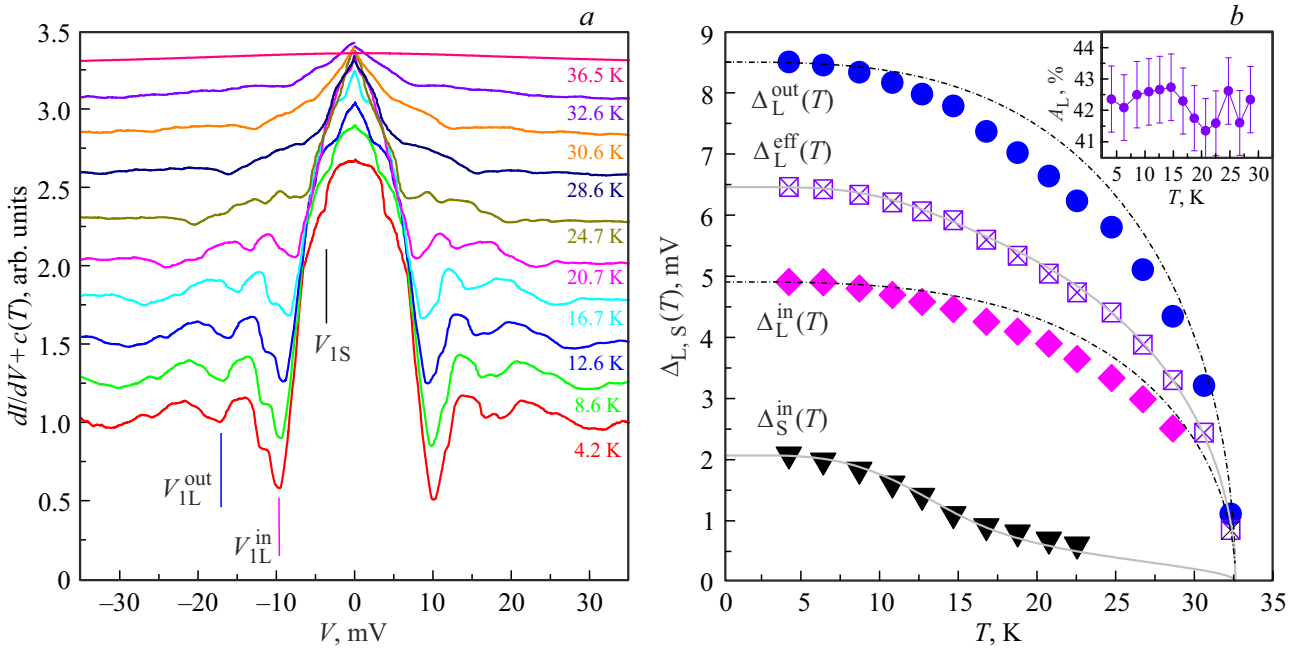

Figure 3. *a* —$dI(V)/dV$-spectra of SnS-Andreev contact formed in polycrystalline $CaKFe_4As_4$ sample, measured at $T = 3.1-33.8$ K. For convenience, $dI(V)/dV$ are normalized to the corresponding spectrum at $T > T_c$ and manually shifted vertically. Vertical dashes at $T = 3.1$ K mark the position of the fundamental Andreev harmonics Δ_{1L}^{out}, Δ_{1L}^{in} and Δ_{1S} of the SC order parameters $2\Delta_L^{out}(0) \approx 17$ meV, $2\Delta_L^{in}(0) \approx 10$ meV, $2\Delta_S(0) \approx 4$ meV. *b* — temperature dependences of SC order parameters $\Delta_L^{out}(T)$, $\Delta_L^{in}(T)$ and $\Delta_S^{in}(T)$ (circles, rhombuses and triangles, respectively). The dependence of the effective large SC gap, estimated as $\Delta_L^{eff}(T) \equiv \sqrt{\left(\Delta_L^{in}(0)\Delta_L^{out}(0)\right)}\delta_L^{out}(T)$, is shown in squares. Solid lines — approximation by a two-band BCS-like model with strong coupling corrections. The inset shows the degree of the estimated anisotropy of the large gap $A_L \equiv 100\,\%\,[1 - \Delta_L^{in}/\Delta_L^{out}]$ depending on the temperature.

There is a feature at small bias $|\Delta_{1S}(0)| \approx 4$ mV, whose position does not correspond to the $n = 2$ subharmonics of the assumed extremes of the large gap and has a fundamentally different temperature dependence (see below). This feature can be interpreted as a fundamental harmonic of a small SC gap $\Delta_S(0) \approx 2$ meV. Such doublets of a small SC order parameter are not observed in the $dI(V)/dV$-spectra of SnS contacts obtained by us. At the same time, on average, the amplitude of the SGS dips of a small SC gap is several times lower compared to intense minima from Δ_L. This can be caused either by the shorter mean free path of the carriers or by strong inelastic scattering in bands with a small SC gap, or by its strong anisotropy (with the possible presence of nodes) in the momentum space. It is also known that the amplitude of the features in the dynamic conductance spectra of Andreev contacts is proportional to the concentration of Cooper pairs [16,18]. Such a small amplitude indicates a small concentration of Cooper pairs, thus corresponding to a small concentration of conduction electrons above T_c in the bands where a small gap developed.

The temperature dependences of the three SC-order parameters directly determined using the data in Figure 3, *a* are shown in Figure 3, *b*. As for the SnS contact discussed above (Figure 2, *b*), the dependences of the assumed extremes of the anisotropic large SC gap $\Delta_L^{out}(T)$ and $\Delta_L^{in}(T)$ (circles and diamonds in Figure 3, *b*) generally repeat the single-band BCS-shaped behavior (the dotted lines in Figure 3, *b*), but run slightly lower. The degree of assumed anisotropy Δ_L in *k*-space $A_L \approx 42\,\%$ almost does not change with increasing temperature up to T_c (within error limits $\pm 1\,\%$), as shown in the insert to Figure 3, *b*. The small SC gap $\Delta_S(T)$ (triangles in Figure 3, *b*) begins to close more rapidly at temperatures of $T \approx 10-15$ K, then smoothly stretches to T_c, forming a „tail“.

Similar temperature behavior of the large and small SC gap, according to Refs. [31–33] is typical for the case of relatively weak interband interaction of SC condensates in *k*-space. The „effective“ isotropic large SC gap $\Delta_L^{eff}(T)$ was used as a rough estimate for approximation of the directly obtained temperature dependences $\Delta_L^{out}(T)$, $\Delta_L^{in}(T)$ and $\Delta_S(T)$ with a model based on the Moskalenko and Suhl equations [18–20] with strong coupling corrections [33]. Taking into account the similar temperature trend $\delta_L^{out}(T) \approx \delta_L^{in}(T) \equiv \delta_L(T)$ (where $\delta(T) \equiv \Delta(T)/\Delta(0)$), the temperature dependence $\Delta_L^{eff}(T)$, shown by squares in Figure 3, *b*, was estimated as $\delta_L^{eff}(T) \equiv \delta_L(T)$, and its low-temperature value — as $\Delta_L^{eff}(0) \equiv \sqrt{\left(\Delta_L^{out}(0)\Delta_L^{in}(0)\right)}$. As can be seen from Figure 3, *b*, the theoretical curves (solid lines) accurately describe the data $\Delta_L^{eff}(T)$ and $\Delta_S(T)$ over the entire temperature range. The local critical contact temperature $T_c^{local} \approx 32.6$ K was estimated as the temperature at which the approximate $\Delta_L^{eff}(0)$ and $\Delta_S(T)$ dependences vanish.

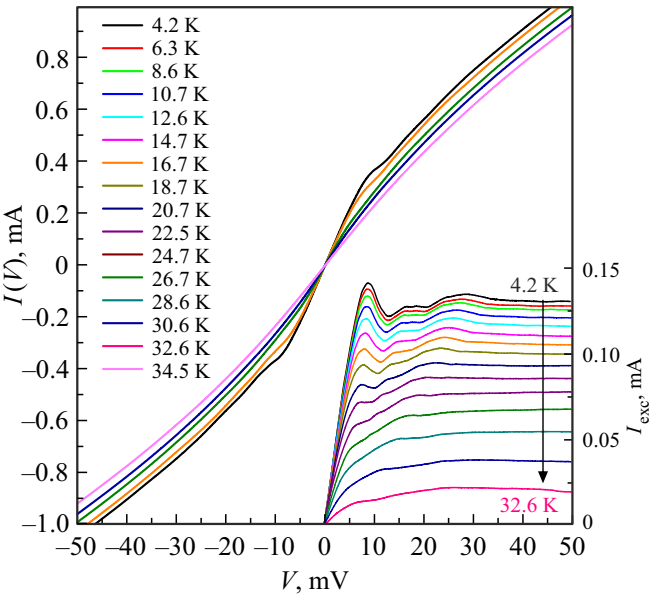

Figure 4. CVC of the SnS-Andreev contact based on polyrystalline $CaKFe_4As_4$, measured at $T = 4.2-34.5$ K. The insert shows the Andreev excess current $I_{exc}(V) \equiv I(V, T) - I(V, T_c)$ at various temperatures.

These smooth approximation curves (solid lines in Figure 3, *b*) were further used as temperature dependences of large and small gaps to analyze the dependences $I_c(T)$, $I_{exc}(T)$ and $G^A_{ZBC}(T)$ within the framework of the two-band approximation proposed above using the formulas (2), (6)–(7), respectively. Thus, we maintained the characteristic ratios $2\Delta_i(0)/k_BT_c$ obtained from the IMARE experiment, and the only fitting parameter was the weight coefficient.

Figure 4 shows a change in the CVC of the same SnS contact (Figure 3) with increase of the temperature. The CVC measured at $T = 34.5\,\text{K} > T_c^{local}$ is almost smooth and does not contain Andreev features. Based on the $I(V, T)$ data, the inset to Figure 4 shows the dependences of the Andreev excess current $I_{exc}(V)$ at various temperatures, determined as the difference between $I(V, T < T_c)$ and the CVC in the normal state $I(V, T = 34.5\,\text{K})$, shown in light pink. The well-marked features of $I_{exc}(V)$ at small bias correspond to the Andreev harmonics on the $dI(V)/dV$-spectrum (Figure 3, *a*), and at large bias $|eV| > 2\Delta_L^{out}(T)$ the excess current tends to a constant value according to the predictions [15,16] and indicating the ballistic mode of the quasiparticle transport ($R_N(T) \approx$ const). As the temperature increases, the Andreev excess current decreases at large bias, turning to zero above T_c^{local} at all bias V.

The normalized temperature dependence of the Andreev excess current $I_{exc}(T)/I_{exc}(0)$ is shown by circles in Figure 5, *a*. To account for the fixed bias $eV = 50$ meV, at which the excess current value was taken at all temperatures, the values of $I_{exc}(T)$ were also normalized to $\tanh[eV/(k_BT)]$ in accordance with the formula (4). The limit cases $\phi = 0, 1$ are shown in Figure 5, *a* with dotted and dashed lines. The experimental dependence $I_{exc}(T)/I_{exc}(0)$ is described by the formula (6) in the best way (gray solid

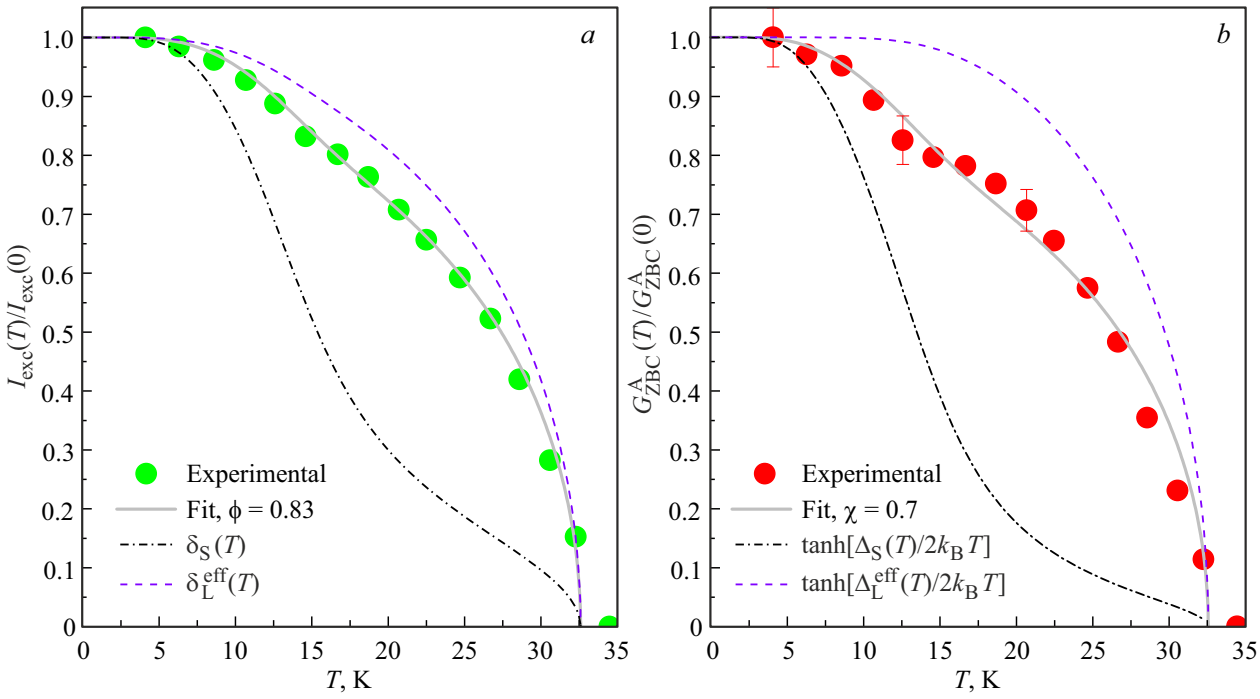

Figure 5. Temperature dependences of Andreev zero-bias conductance (*a*) and Andreev excess current (*b*) according to Figure 4. The limit cases $\phi, \chi = 1$ and $\phi, \chi = 0$ based on the approximation curves $\Delta_L^{eff}(T)$ and $\Delta_S(T)$ (Figure 3, *b*) are shown as dashed and dotted lines, respectively; approximations formulas (6), (7) — solid lines.

Weight coefficients ϕ, ω, χ — contribution of bands with a large SC gap to the dependence of the Andreev excess current, critical SC current and Andreev zero-bias conductance, respectively. The contributions of bands with Δ_L^{eff} to the total conductance of χ_{exc} and χ_{Ic}, estimated from $I_{exc}(T)$ and $I_c(T)$ data, respectively are given for comparison

$I_{exc}(T)$ data		$I_c(T)$ data		$G^A_{ZBC}(T)$ data
ϕ	χ_{exc}	ω	χ_{Ic}	χ
0.79–0.87	**0.54–0.67**	0.94–0.98	**0.83–0.94**	**0.68–0.72**

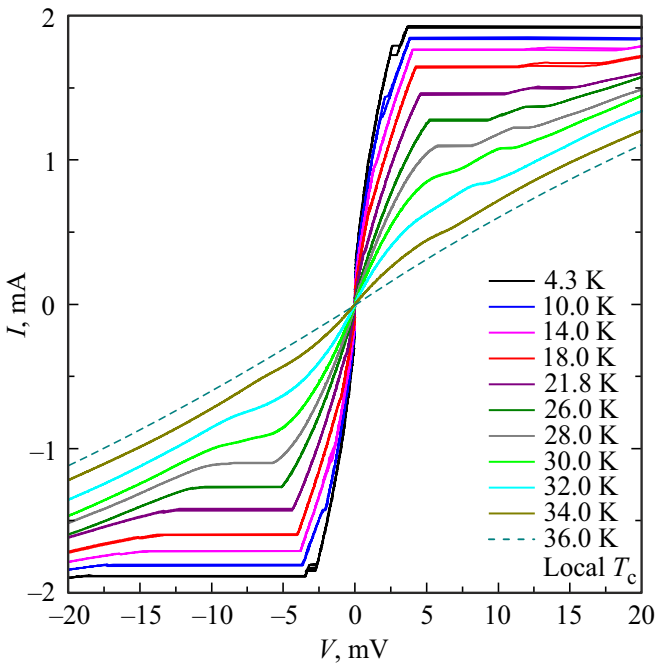

Figure 6. CVC of a superconducting short-circuit connected in series with a SnS-Andreev contact formed in a polycrystalline $CaKFe_4As_4$ sample and measured in the range of $T = 4.3–36.0$ K. The current plateaus on the CVC correspond to the critical currents of the transition of the SC short circuit to the normal state with a finite resistance. The dashed line shows the CVC of this tunneling contact in the normal state at local $T_c = 36.0$ K.

line in Figure 5, *a*) with a weight coefficient $\phi = 0.82$, thus, the contribution of bands with an effective large gap to the total conductance, according to the coefficient conversion formula (10), can be estimated using the values $\Delta_L^{eff}(0)$ and $\Delta_S(0)$ as $\chi_{exc} = 0.64$.

The Andreev zero-bias conductance $G^A_{ZBC}(T)/G^A_{ZBC}(0)$, normalized to its value at $T \ll T_c$, for the same contact is shown in Figure 5, *b* by circles. At temperatures of the order of 12 K, there is a noticeable „curving down“ caused by the contribution of the quasiparticle transport of the bands with the small SC gap and its suppression by inelastic scattering with an increase of T. The obtained dependence can be described in the framework of the two-band approximation (7), with the estimated partial contribution of the „leading“ zone with a large SC gap $\chi = 0.7$ (solid line in Figure 5, *b*).

Figure 6 shows a family of CVC in the temperature range of $T = 4.3–36.0$ K of a hybrid tunneling junction consisting of SC short circuit (ScS) connected in series with an SnS-Andreev contact. The formation of hybrid tunneling structures in which certain contacts are connected in series or parallel becomes possible when using the break-junction technique on polycrystalline samples. A similar type of CVC in which the low-bias part tends, but does not reach the vertical, at a certain critical current I^* „jumps “ to a current plateau, and at high currents (see CVC measured at $T = 4.3$ K in a wide bias range, in the insert to Figure 7, *a*) demonstrates an excess current compared to the CVC in the normal state (dashed line in Figure 6), is typical for the case when the resistance of a series-connected SnS contact is $R_N^{SnS} \ll R_N^{ScS}$. It should be noted that when the SnS and ScS contacts are connected in series, it is impossible to observe a strictly vertical supercurrent branch. Nevertheless, in the current source mode, a change in the value of the „jump“ current with a temperature of $I^*(T)$ allows obtaining a temperature dependence of the critical current of the superconductor, which is approximately proportional to the concentration of Cooper pairs. Starting from $T = 30$ K, $I^*(T)$ was defined as the current at which the minimum of the derivative $dI(V)/dV$ is observed.

A similar dependence $I^*(T) \equiv I_c(T)$, obtained from Figure 6, is shown in Figure 7, *a* with blue triangles. For comparison, the circles show a similar relationship for a sequential ScS-SnS structure obtained on another $CaKFe_4As_4$ sample from the same batch. A similarity of their shape is observed. The solid lines correspond to a simplified theoretical approximation $I_c(T)$ using two terms based on BCS-shaped dependencies $\Delta(T)$, while using only one term does not allow a qualitative description of the experimental data. It can be seen that both approximations tend to $T_c \approx 36.3–36.7$ K, which is in excellent agreement with $R(T)$ of the bulk sample shown in Figure 7, *a* by open circles.

We have obtained several experimental dependencies $I^*(T)$, and the data shown in Figure 7, *b* in normalized coordinates is a representative sample of these results. Good reproducibility is visible. Figure 7, *b* contains both sets of data from the panel Figure 7, *a*, the type of symbols is preserved. We have approximated these dependencies within the framework of the expression (2); based on the definitions (3), (9), It can be concluded that the weighting factor ω for the dependency $I_c(T)$ should correspond to the weighting factor ϕ for the dependency $I_{exc}(T)$. As a

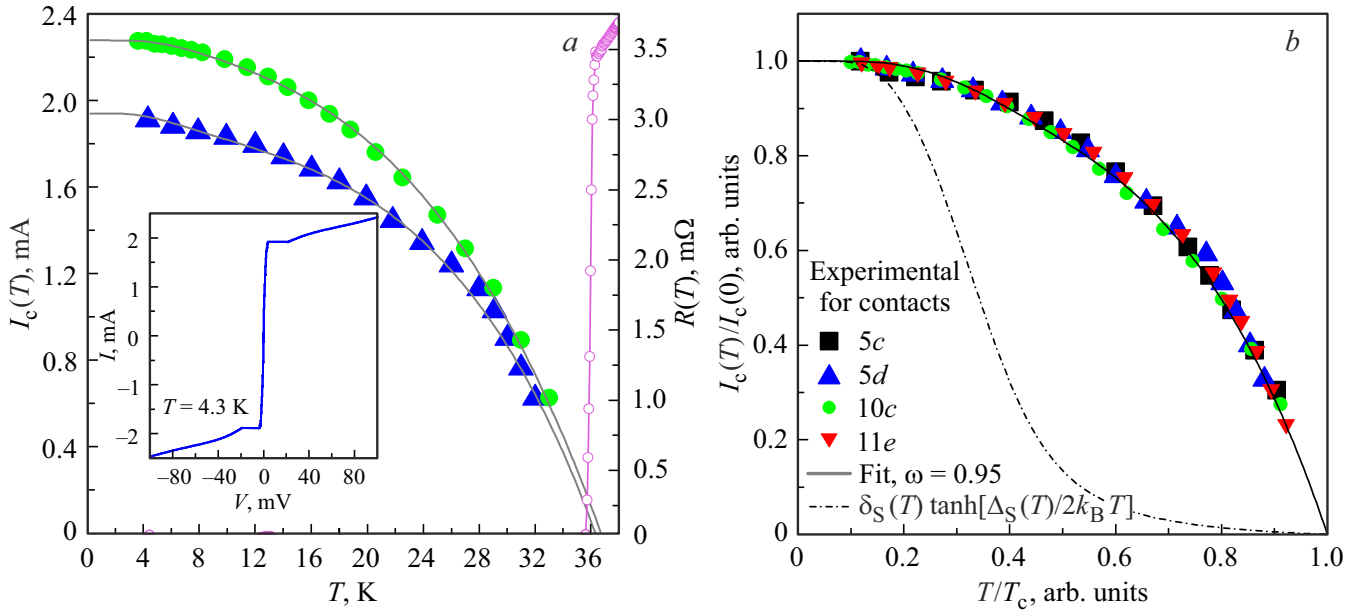

Figure 7. *a* — temperature dependences of the critical current for two short circuits based on $CaKFe_4As_4$ (left axis). The dependence constructed from the data in Figure 6 is shown by blue triangles; solid lines — simplified theoretical approximation $I_c(T)$. Light circles — the dependence of the volumetric resistance of the sample on the temperature $R(T)$ in the region of transition to the SC state (right axis). The insert shows the CVC of the tunneling contact from Figure 6 at $T = 4.3$ K over a wide range of bias voltages. *b* — dependence of the critical current on temperature in normalized coordinates. In addition to the experimental data from the panel „a“, the red triangles and black squares show $I_c(T)/I_c(0)$ data for two other contacts based on polycrystalline $CaKFe_4As_4$ samples. The limiting case $\omega = 0$ based on the approximation curve $\Delta_S(T)$ (Figure 3, *b*) is shown by a dotted line, the approximation by formula (2) is shown by a solid line.

result, the estimated range of ω was 0.94–0.98 (Figure 7, *b*), however, the correspondence of ω and ϕ is not observed. Possible reasons for this are discussed below.

4. Discussion

For ease of comparison, the obtained weight coefficients ω, χ_{Ic}, as well as ϕ, χ_{exc} and χ are shown in the table.

Thus, the contribution of bands with a large SC gap to the overall conductance was estimated in three ways: directly as a weighting factor χ for the dependence $G^{A}_{ZBC}(T)$, and also using coefficients ϕ and ω, by recalculation using the formula (9); the values are denoted as χ_{exc} and ω_{Ic}, respectively. The obtained ranges of values χ_{exc} and χ turned out to be close, which indicates the qualitative consistency of estimates of the partial conductance of the effective band with a large SC gap in the normal state based on an analysis of the temperature behavior of the features caused by IMARE. The correspondence of the estimates χ_{Ic} and χ turned out to be worse, their ranges do not overlap, which may indicate an oversimplification of expression (2), which does not take into account the ratio of the geometric dimensions of the contact with the London penetration depth, as well as the steaming effect of critical current densities.

In general, comparing the values of χ_{exc}, χ_{Ic} and χ, it is possible to conclude that the contribution of effective bands with a large SC gap to the overall conductance of $CaKFe_4As_4$ is dominant.

It should be noted that the isotropic double-term approximation used is based on the formulas (2), (6), (7) is a serious simplification, which limits its application to the study of multiple-band transport in such a complex system as $CaKFe_4As_4$ [3]. Nevertheless, the estimate χ_{exc}, obtained on the basis of the Andreev excess current analysis, seems to be the most physically correct in this case. Here are some arguments in favor of this statement.

The features of the small SC gap are almost indistinguishable in the dI/dV-spectra in Figures 1–3, which creates certain difficulties in studying this order parameter. On the one hand, as mentioned above, this may be caused by the low concentration of Cooper pairs in the corresponding bands. The latter is confirmed by the data in the table, especially the results of the approximation of the dependencies $I_c(T)$ (shown in Figure 7, *b*), which correspond to a small contribution from bands with a small gap, on average less than 12 %. Another factor suppressing the amplitude of features from a small SC gap in the $dI(V)/dV$-spectra of SnS contacts may be its strong anisotropy in k-space, including the presence of nodes in the distribution [22,23]. In the latter case, the parameter determined in the IMARE experiment is of the order $\Delta_S \equiv \Delta_S^{out}$, and $\Delta_S^{in} \to 0$. In this case, we should expect a decrease in the weight coefficients ω and χ, while the

approximation $I_{exc}(T)$ and the weight coefficient ϕ will not change.

Inelastic scattering, which smears the gap peaks of the density of electronic states, according to the approach [19,20], practically does not affect $I_{exc}(T)$, while dominating the dynamics of Andreev processes precisely in the foot region, limiting its height, i. e., the value of Andreev zero-bias conductance G^{A}_{ZBC}. Taking into account the increase in $\Gamma(T)/\Delta(T)$ with temperature, which is not considered in the approach [19,20], we should expect a faster decrease in $G^{A}_{ZBC}(T)$ near T_c compared with the predictions of formula (7). Finally, a small, but nonzero value of the barrier parameter Z, according to Ref. [15], affects only the absolute value of $I_{exc}(0)$, without changing its temperature dependence.

Summarizing the above, the approximation of $I_{exc}(T)$ and the estimated weighting factor ϕ seem to be the most „stable“ relative to taking into account the additional parameters of a real SnS contact based on $CaKFe_4As_4$. At the same time, it is necessary to expand the existing theoretical concepts described in Refs. [19,20] for a correct description of $G^{A}_{ZBC}(T)$ and the development of new models predicting the temperature behavior of $I_c(T)$ for the case of planar contact or small-thickness SC short circuit in a layered superconductor.

Thus, the contribution of the bands with a large SC gap to the overall conductance can be estimated as $\chi_{exc} \approx 0.54-0.67$. This value is close to $\chi_{122} \approx 0.5$, previously estimated using IMARE spectroscopy [21] and infrared Fourier spectroscopy [34] in related pnictides $Ba(Fe,Ni)_2As_2$ of 122 family.

5. Conclusions

The magnitudes and temperature dependences of microscopic superconducting order parameters $\Delta_i(T)$ were determined by analyzing the features of $I(V)$ and $dI(V)/dV$-characteristics of various tunneling structures created in polycrystalline $CaKFe_4As_4$ samples, as well as the dependence of Andreev excess current $I_{exc}(T)$, Andreev zero-bias conductance $G^{A}_{ZBC}(T)$ and supercurrent on the temperature $I_c(T)$. Based on the three-method evaluation of the partial conductances of the two effective bands, which utilized directly measured $\Delta_i(T)$ and a comparison of the obtained results, the contribution of the bands with the large superconducting gap to the total conductance was estimated to be $\approx 54-67\,\%$.

Acknowledgments

This study was supported by the Russian Science Foundation, project No. 24-72-10109. The measurements were partially carried out using the equipment of the Lebedev Physics Institute's Collective Use Center of the Russian Academy of Sciences.

Conflict of interest

The authors declare that they have no conflict of interest.

References

[1] A. Iyo, K. Kawashima, T. Kinjo, T. Nishio, S. Ishida, H. Fujihisa, Y. Gotoh, K. Kihou, H. Eisaki, Y. Yoshida. J. Am. Chem. Soc. **138**, 3410 (2016).
[2] G. Mebratie, T. Negussie, G. Kahsay. Nano Select, 0:e202400124 (2024).
[3] F. Lochner, F. Ahn, T. Hickel, I. Eremin. Phys. Rev. B **96**, 094521 (2017).
[4] D. Mou, T. Kong, W.R. Meier, F. Lochner, L.-L. Wang, Q. Lin, Y. Wu, S.L. Bud'ko, I. Eremin, D.D. Johnson, P.C. Canfield, A. Kaminski. Phys. Rev. Lett. **117**, 277001 (2016).
[5] W. Liu, L. Cao, S. Zhu, L. Kong, G. Wang, M. Papaj, P. Zhang, Y.-B. Liu, H. Chen, G. Li, F. Yang, T. Kondo, S. Du, G.-H. Cao, S. Shin, L. Fu, Z. Yin, H.-J. Gao, H. Ding. Nature Commun. **11**, 5688 (2020).
[6] R. Yang, Y. Dai, B. Xu, W. Zhang, Z. Qiu, Q. Sui, C.C. Homes, X. Qiu. Phys. Rev. B **95**, 064506 (2017).
[7] S.Z. Zhao, H.-Y. Song, L.L. Hu, T. Xie, C. Liu, H.Q. Luo, C.-Y. Jiang, X. Zhang, X.C. Nie, J.-Q. Meng, Y.-X. Duan, S.-B. Liu, H.-Y. Xie, H.Y. Liu. Phys. Rev. B **102**, 144519 (2020).
[8] K. Cho, A. Fente, S. Teknowijoyo, M.A. Tanatar, K.R. Joshi, N.M. Nusran, T. Kong, W.R. Meier, U. Kaluarachchi1, I. Guillamon, H. Suderow, S.L. Bud'ko, P.C. Canfield1, R. Prozorov. Phys. Rev. B **95**, 100502(R) (2017).
[9] L. Cao, Y. Song, Y.-B. Liu, Q. Zheng, G. Han, W. Liu, M. Li, H. Chen, Y. Xing, G.-H. Cao, H. Ding, X. Lin, S. Du, Y.-Y. Zhang, G. Li, Z. Wang, H.-J. Gao. Nano Research **14**, 3921 (2021).
[10] A. Fente, W.R. Meier, T. Kong, V.G. Kogan, S.L. Bud'ko, P.C. Canfield, I. Guillamon, H. Suderow. Phys. Rev. B **97**, 134501 (2018).
[11] E. Piatti, D. Torsello, F. Breccia, T. Tamegai, G. Ghigo, D. Daghero. Nanomaterials **14**, 1319 (2024).
[12] P.K. Biswas, A. Iyo, Y. Yoshida, H. Eisaki, K. Kawashima, A.D. Hillier. Phys. Rev. B **95**, 140505(R) (2017).
[13] R. Khasanov, W.R. Meier, Y. Wu, D. Mou, S.L. Bud'ko, I. Eremin, H. Luetkens, A. Kaminski, P.C. Canfield, A. Amato. Phys. Rev. B **97**, 140503(R) (2018).
[14] V. Ambegaokar, A. Baratoff. Phys. Rev. Lett. **10**, 486 (1963).
[15] M. Octavio, M. Tinkham, G.E. Blonder, T.M. Klapwijk. Phys. Rev. B **27**, 6739 (1983).
[16] R. Kümmel, U. Gunsenheimer, R. Nicolsky. Phys. Rev. B **42**, 3992 (1990).
[17] Z. Popovic, P. Miranovic. Eur. Phys. J. Plus **138**, 767 (2023).
[18] Z. Popovic, S.A. Kuzmichev, T.E. Kuzmicheva. J. Appl. Phys. **128**, 013901 (2020).
[19] U. Gunsenheimer, A.D. Zaikin. Phys. Rev. B **50**, 6317 (1994).
[20] U. Gunsenheimer, A.D. Zaikin. Europhys. Lett. **41**, 195 (1998).
[21] T.E. Kuzmicheva, S.A. Kuzmichev, K.S. Pervakov, V.A. Vlasenko. JETP Lett. **112**, 786 (2020).
[22] T.P. Devereaux, P. Fulde. Phys. Rev. B **47**, 14638 (1993).
[23] S.A. Kuzmichev, T.E. Kuzmicheva. Low Temp. Phys. **42**, 1008 (2016).
[24] J. Moreland, J.W. Ekin. J. Appl. Phys. **58**, 3888 (1958).

[25] T.E. Kuzmicheva, S.A. Kuzmichev, K.S. Pervakov, V.A. Vlasenko. JETP Letters **118**, 514 (2023).
[26] T.E. Kuzmicheva, S.A. Kuzmichev, N.D. Zhigadlo. Phys. Rev. B **100**, 144504 (2019).
[27] S.A. Kuzmichev, K.S. Pervakov, V.A. Vlasenko, A.Yu. Degtyarenko, S.Yu. Gavrilkin, T.E. Kuzmicheva. JETP Letters **116**, 723 (2022).
[28] T. Kuzmicheva, K. Pervakov, V. Vlasenko, A. Degtyarenko, S. Kuzmichev. J. Supercond. Novel Magn. **37**, 379 (2024).
[29] S. Kuzmichev, T. Kuzmicheva, I. Morozov, A. Boltalin, A. Shilov. SN Appl. Sci. **4**, 189 (2022).
[30] S.A. Kuzmichev, I.V. Morozov, A.I. Shilov, Ye.O. Rakhmanov, T.E. Kuzmicheva. JETP Lett. **120**, 125 (2024).
[31] V.A. Moskalenko. Phys. Met. Metallogr. **8**, 25 (1959).
[32] H. Suhl, B.T. Matthias, L.R. Walker. Phys. Rev. Lett. **3**, 552 (1959).
[33] T.E. Kuzmicheva, S.A. Kuzmichev. Low Temp. Phys. **45**, 1161 (2019).
[34] Yu.A. Aleshchenko, A.V. Muratov, G.A. Ummarino, S. Richter, A.A. Thomas, R. Hühne. J. Phys.: Condens. Matter. **33**, 045601 (2021).

Translated by A.Akhtyamov